

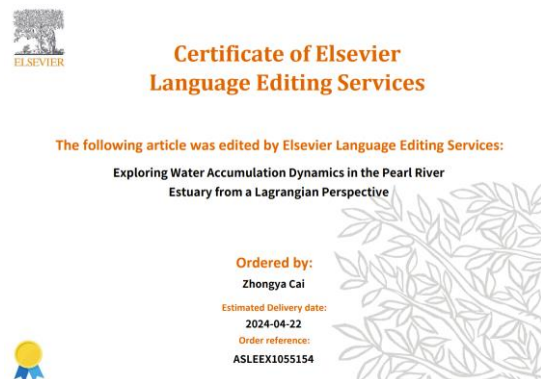
This paper investigates seasonal patterns of water particles accumulation in Pearl River Estuary subregions following a Lagrangian approach. The authors determined flow fields using an Eulerian model and then monitored particles trajectories for 30 days in the summer and 30 days in the winter by implementing a 3D Lagrangian model. Their main conclusion is that plume fronts and velocity convergence are important factors in the determination of water accumulation dynamics while they also identify a negative correlation between divergence and accumulation probability. I reckon that the manuscript contains work that is worthy to be published but it also needs considerable improvements before this happens. Main concerns have to do with phrasing, figures quality and inadequate information supplied. I provide the following general and specific comments which hopefully the authors will find useful and constructive.

Response: Thanks for your insightful suggestions and comments, which help to improve our work. We carefully revised our manuscript based on your suggestions and listed our responses as follow.

General comments

1. The manuscript needs a thorough revision in terms of language. Specifically, the use of present tense throughout the manuscript is recommended instead of past tense.

Response: Thanks for your suggestions. We made a thorough language editing in the revised manuscript. And we use present tense instead of past tense in the modified manuscript.



2. A more detailed description of the PRE dynamics is demanded so that the reader can appreciate the unique and complex physical processes in this ecosystem. For instance, the fact that the river discharge in the PRE is higher in the summer and lower in the winter is counterintuitive as in most systems, discharges are higher during winter due to increased rainfall and runoff. It is therefore recommended to the authors to mention this specifically in their introduction. In addition, the monsoonal cycles need to be mentioned as they are important for the water circulation. Relevant information could be included in a separate paragraph either at the end of the Introduction or at the start of section 2.

Response: Thanks for the suggestion. In the revised manuscript, we provide a more detailed description of the PRE dynamics in Line 26-47 in introduction, including the tidal currents, river discharge and wind forcing.

The Pearl River Estuary (PRE), located in the northern South China Sea (NSCS) (Fig. 1a), is influenced by the East Asian Monsoon, with northeasterly winds prevailing in winter and southwesterly winds prevailing in summer (T. Li & Li, 2018). Thus, in the PRE, winter is characterized as a dry season, and summer is characterized as a wet season due to the large rainfall induced by the moist air brought from the South China Sea; consequently, the river discharge in summer ($\sim 20,000 \text{ m}^3\text{s}^{-1}$) is approximately five times more than that in winter ($\sim 3,600 \text{ m}^3\text{s}^{-1}$) (Harrison, Yin, Lee, Gan, & Liu, 2008). This is quite different from many other river deltas, such as the Mississippi deltas, where river discharge reaches a maximum in winter and spring, but is reduced in summer and autumn (Lane et al., 2007).

As a bell-shaped estuary, the width increases from approximately 5 km at the upper end to 35 km at the lower end. Despite the two narrow, deeper channels ($\sim 20 \text{ m}$ in depth), the PRE is shallow, with a water depth of approximately 2-10 m. The PRE is a partially mixed estuary in which circulation is jointly controlled by river discharge, tides, wind, and topography (Ascione Kenov, Garcia, & Neves, 2012; Banas & Hickey, 2005; Gong, Shen, & Hong, 2009; C. He, Yin, Stocchino, & Wai, 2023; C. He, Yin, Stocchino, Wai, & Li, 2022; Liu, Zu, & Gan, 2020). There are two distinct dynamic regimes in the PRE. The narrow upper part of the PRE shows classical gravitational circulation, whereas in the wider lower part of the PRE, where the Coriolis effect becomes essential, the topography and interaction with the monsoon-driven shelf current complicate the circulation (Dong, Su, Ah Wong, Cao, & Chen, 2004; Wong et al., 2003; Zu & Gan, 2015). Gravitational circulation occurs in the two deep channel regions, whereas currents show precise seasonal characteristics over the shallower western estuary. Geostrophic wind-driven coastal currents intrude into the PRE during the summer upwelling season (Zu & Gan, 2015), whereas seaward buoyancy-driven coastal currents flow out of the PRE during winter (Dong et al., 2004; Wong et al., 2003). The alternation of the spring-neap tide and variation in river discharge play crucial roles in modulating stratification and mixing inside the PRE (Mao, Shi, Yin, Gan, & Qi, 2004; Pan, Lai, & Thomas Devlin, 2020; Zu, Wang, Gan, & Guan, 2014). Strong tidal mixing in the middle PRE has led to the conversion of estuarine river plumes into buoyancy-driven coastal currents (Dong et al., 2004; Zu et al., 2014).

3. A deeper insight is demanded when discussing the results, particularly on the inter-play among the three basic physical mechanisms of gravitational circulation, tidal and shelf currents in the estuary. It is generally not a good practice to merge results with discussion. It is recommended to detach discussion from section 3 and put it in a separate paragraph. In this way, the core messages of this work can be better illustrated.

Response: Thank you for the comment. In the revised manuscript, we have separated the Discussion from the Results. Following the reviewer's suggestion, changes in circulation and density structure were examined to gain a deeper understanding of the influences of river-induced gravitational circulation, tidal effects, and shelf currents.

As the tidal current affects the intensity of mixing in the water column, once removed, the offshore motion in the UPPER region is reduced in both summer and winter. During winter, the intrusion water from the shelf moves straight landward and arrives at the upper part of the estuary. Along the transect of AB (Figure R1a), we further checked the changes in the density stratification and vertical structure of circulation (Figure R2). The intensification and landward movement of the bottom

intrusion is associated with the stronger density stratification. The removal of the tidal current leads to weaker mixing and intensified stratification, as also revealed in previous studies where weaker tide intensity contributed to increased stratification in the PRE (e.g., Pan et al. (2020)).

Consequently, when the tidal currents were removed in summer, the accumulation probability in the midwestern region increased (Figure 7a in the original manuscript), whereas, during winter, the intensified onshore intrusion led to a higher accumulation in the UPPER region (Figure 7b in the original manuscript). Thus, the tidal current mainly resists bottom intrusion water in the midwestern estuary by changing the mixing intensity and density structure.

Similarly, we checked the changes in bottom intrusion and density stratification in the river reduction case. With reduced river discharge, the seaward motion in the entire estuary primarily decreased in both winter and summer (Figure R3). Along the AB transect, the landward velocity increases in the upper estuary, and seaward motions are accelerated in the lower estuary during winter (Figure R3d), which is associated with the negative/positive value of the accumulation probability in the middle/lower estuary during winter (Figure 8b in the original manuscript). In summer, reduced stratification leads to a well-mixed water column in the inner estuary, and the landward movement of density to the middle estuary blocks the water in the upper part of the estuary (Figure R3c). As a result, accumulation in the inner estuary increased in summer when river discharge was reduced (Figure 8a in the original manuscript).

Generally, tidal currents and river-induced gravitational circulation affect accumulation in different ways and affect different regions of the estuary. Their joint effects controlled the accumulation pattern. The above explanation was added in the revised manuscript.

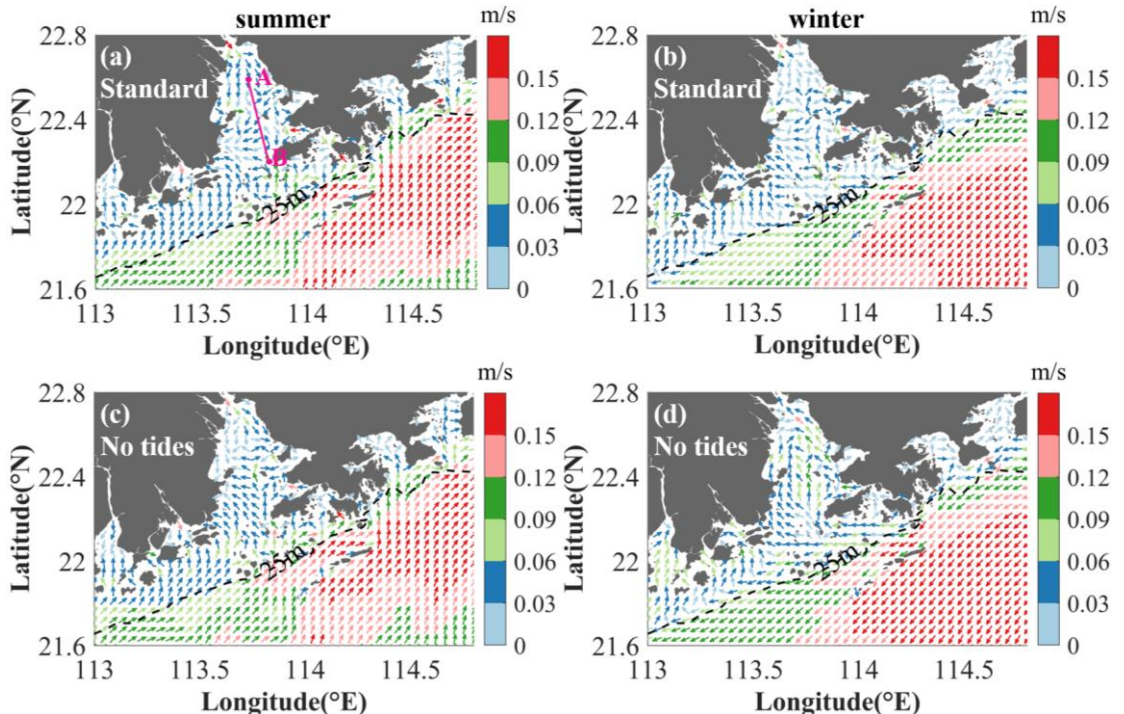


Figure R1. (a-b) The flow field of the standard case at the bottom layer during summer and winter time, respectively. (c-d) are the same as (a-b), except for removing the tidal currents. The colorbar represents the velocity of the current. AB indicates the location of the transect to show the vertical structure.

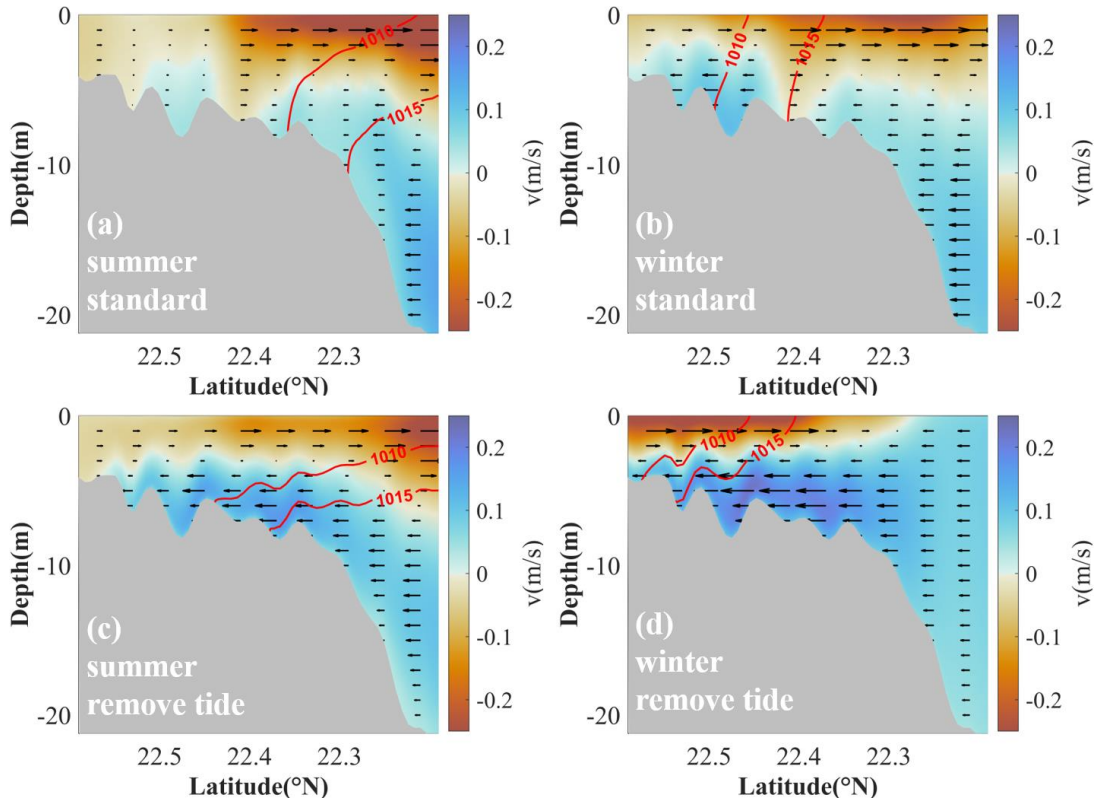


Figure R2. (a-b) The along transect velocity (color and arrow, positive indicate the onshore intrusion) and density contour of 1010 kg/m^3 and 1015 kg/m^3 (red lines) in AB during summer and winter. The location of AB shown in Figure R.1 (c-d) the same as (a-b), except for removing the tidal currents.

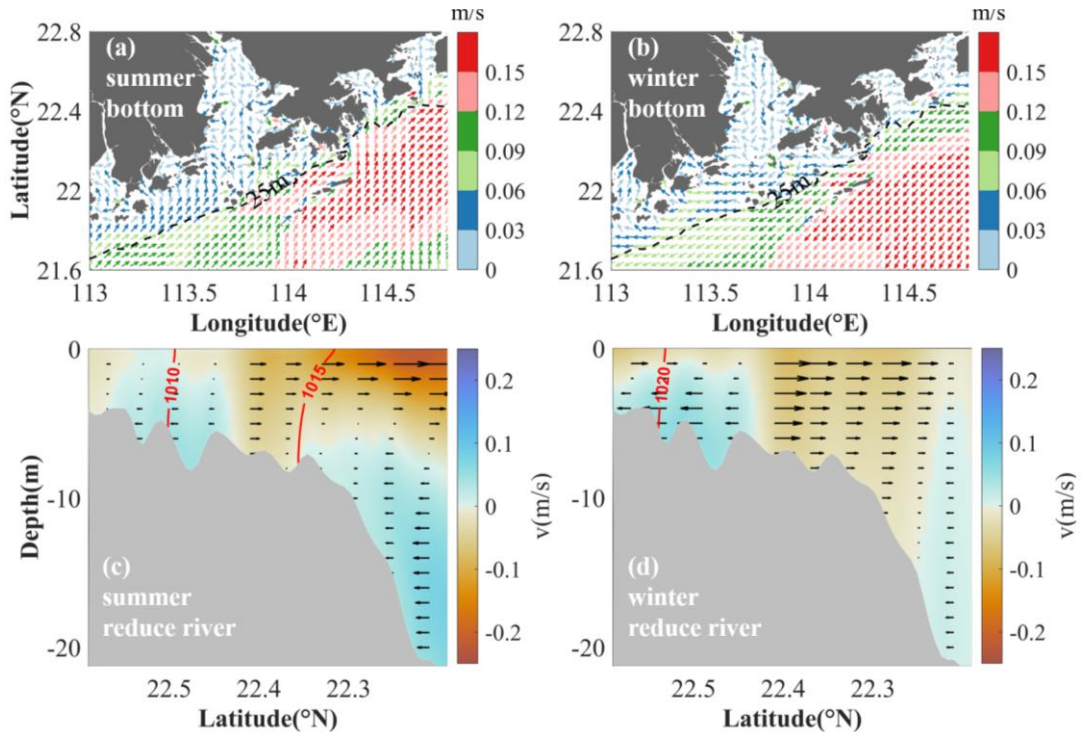


Figure R3: (a-b) The flow field of the river reduced case at the bottom layer during summer and winter time,

respectively. (c-d) The along transect velocity (color and arrow, positive indicate the onshore intrusion) and density contour of 1010 kg/m^3 and 1015 kg/m^3 (red lines) in AB during summer and winter. The location of AB is shown in Figure R1.

4. The results analysis and discussion focus mainly on the influence of river discharge, tide, and plume fronts. But the monsoonal cycles and consequently wind forcing, downwelling, upwelling etc. are also important parameters that affect water circulation and accumulation. These are only briefly mentioned in page 6 (lines 140-142) and somehow their effect is understated in the manuscript. The contribution of the monsoonal climate can be reevaluated and better highlighted.

Response: Following the reviewer's suggestion, an additional experiment was conducted to discuss the impact of wind forcing on circulation patterns. In addition, a deeper analysis was conducted to illustrate better the joint effects of river discharge, wind forcing, and tidal currents on the accumulation pattern in the bottom layer.

Generally, the wind has less influence on the circulation in the estuary (Figure R4). In summer, compared with the river and tide, the wind does not have a significant impact on circulation in the estuary. Only the shelf current outside the estuary was weakened (Figure R4a, c). In winter, the wind mainly affects the current in the lower estuary and adjacent shelf, where offshore motions are reduced, and landward transport to the south of the WEST region is strengthened (Figure R4b, c).

Consequently, the accumulation pattern and connection among subregions remain the similar to standard case in summer. In winter, higher accumulations occurred mainly along the west side of the estuary (Figure R5b). The strengthened westward current and reduced offshore motion transport more water from Hong Kong and Shelf towards the WEST region (Figure R5d). The connection between other regions is similar to standard case, mainly differences appear in the WEST region.

By comparing the accumulation patterns and circulation under different dynamic factors, we summarized the relationships among the three controlled factors. In summer, the circulation and accumulation in the estuary are mainly controlled by river and tidal currents, which together contribute to accelerating the offshore motion in most regions. Compared with tidal currents and river discharges, the wind has less impact. In winter, the existence of tidal currents and river discharge leads to the convergence of water parcels in the WEST region and divergence in the UPPER region. Wind mainly affected the shelf current and accelerated the offshore transport on the western side of the lower estuary.

Since the effect of the wind in the estuary is relatively small, we did not put this additional case in the manuscript. In the revised manuscript, we clarify the influence of wind forcing:

Line 267-269: "The tides and rivers had essential influences on the estuarine circulation and associated mass transport in the PRE, whereas the wind mainly affected the shelf current and had less influence on the mass accumulation inside the estuary (figures not shown here)."

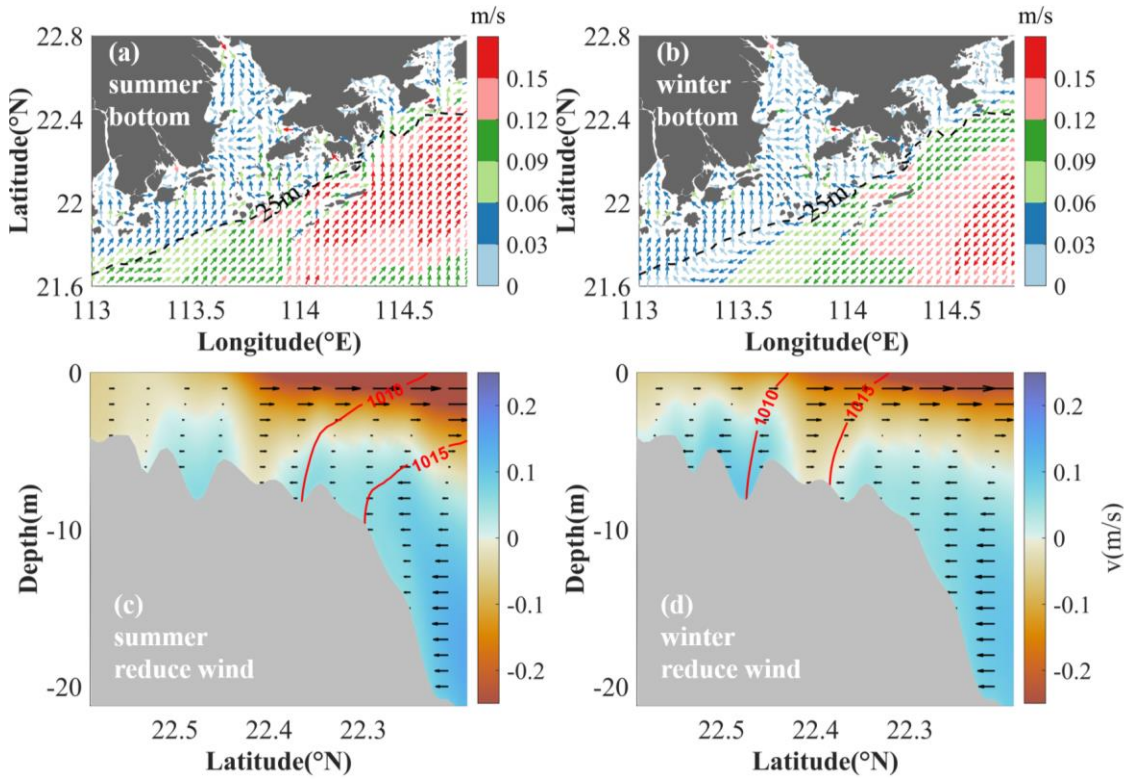


Figure R4. The flow field of reduced wind forcing at the bottom layer in summer (a) and winter (b), respectively. The flow field of reduced wind forcing in transect AB at the bottom layer in summer (c) and winter (d), respectively. The colorbar represents the onshore velocity, and the positive value means the landward motion in transect AB. The arrow represents the current direction, and the length represents the strength of the currents. The red line represents the isopycnal of 1010 kg/m^3 and 1015 kg/m^3 .

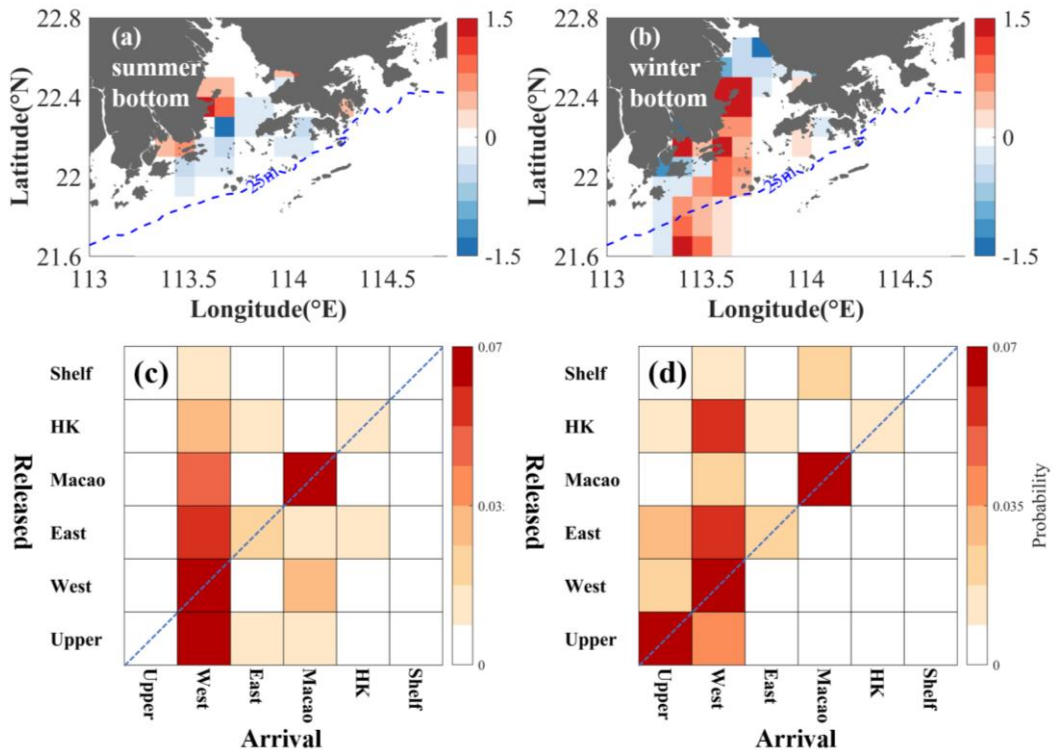


Figure R5. Accumulation probability at the bottom layer during summer (a) and winter (b). The colorbar indicate the magnitude of accumulation probability. (c-d) The connection between the six subregions is when the wind force is reduced during the summer and winter, respectively. The horizontal and vertical axes represent the arrival and release regions, respectively.

5. FontSizes and Figures sizes need to be enlarged.

Response: FontSizes and Figures sizes has been enlarged in the revised manuscript.

Specific comments

Introduction:

Lines 43-46. It would be useful to expand and elaborate on why it is important to know and identify areas of water accumulation. Is this interesting only for the PRE or for any estuary? Is eutrophication the only problem or is it particularly concerning for the PRE? Note also that eutrophication is not an anthropogenic activity but one of its adverse consequences.

The introduction can be enriched with some further literature on the topic. Is this a topic that has been explored before and to what extent?

Response: Thank you for the comment. The estuary is a transition region between the land and ocean and is facing increasing pressure for water protection (Callahan et al., 2004) due to recent intensified human activities. It should be noted that under complicated water motions, water is more likely to be trapped in some regions. For example, the salt wedge provides a sink for pollutants in estuaries (Vermeiren, Muñoz, & Ikejima, 2016), and higher concentrations of microplastics have been observed at the salt wedge in the Rio de la Plata estuary (Acha et al., 2003). The accumulation of fine particles in some estuarine regions with weak flushing traps had high concentrations of heavy metals in them (Balachandran et al., 2005). Therefore, exploring the accumulation dynamics in estuaries provides favorable conditions for revealing the formation of pollutant sinks (Mestres et al., 2006; Tao, Niu, Dong, Fu, & Lou, 2021; Vermeiren et al., 2016; A.-j. Wang et al., 2016).

Eutrophication is not the only concern of PRE. D. Zhang et al. (2013) found that trace elements have the highest concentrations in the western PRE. Microplastics are concentrated in Hong Kong water and the western part of the PRE owing to the influence of tidal currents and the Pearl River outflow (Lam et al., 2020). Tao et al. (2021) revealed that the accumulation of nitrogen and silicate occurred in the upper part of the PRE, and phosphorus pollution was observed in the northeast of the PRE (e.g., Shenzhen Bay). These phenomena are also related to the accumulation patterns in the PRE.

In the previous investigation, the phenomenon of accumulation of pollutants/materials in particular regions were noticed, but do not have a clear understanding of its spatial pattern and underlying physical control. In this study, using the PRE as a typical example, we attempted to determine the connection between different subregions in the PRE to verify the physical processes controlling accumulation patterns.

Following the reviewer's suggestions, we integrate the above information in the revised manuscript:

Line 53-71:

In estuaries, some regions are more likely to attract water because of complicated current circulation,

which can be considered as stronger horizontal convergence targets for some materials (T. Wang et al., 2022). For example, the salt wedge acts as a significant pollutant sink in an estuary, and a higher concentration of microplastics is always obtained at the salt wedge in the Rio de la Plata estuary (Acha et al., 2003; Vermeiren, Muñoz, & Ikejima, 2016). Areas accompanied with higher concentration of nitrogen and phosphorus are usually appearing eutrophic (Tao, Niu, Dong, Fu, & Lou, 2021). Heavy metal pollution in estuaries has been observed in areas that prefer to concentrate fine particles (Balachandran et al., 2005). Therefore, identifying the accumulation areas in estuary-shelf systems provides an adequate estimate for surveying pollutant sinks (Mestres et al., 2006; Tao et al., 2021; Vermeiren et al., 2016; A.-j. Wang et al., 2016).

With intensified human activities, pollutant sinks related to the accumulation phenomena in the PRE have attracted attention. Tao et al. (2021) revealed that the upper part of the PRE is a target sink for nitrogen and silicate. D. Zhang et al. (2013) found that trace elements prefer to accumulate on the PRE's west side. Higher concentrations of microplastics have been observed in western estuaries and Hong Kong waters (Lam et al., 2020). Similarly, studies on hypoxia have shown that the convergence of buoyancy-driven currents and wind-driven shelf flows contributes to the formation of stable water columns, providing favorable conditions for the development of hypoxic zones (e.g., D. Li et al. (2021); X. Li et al. (2020)). The high frequency of hypoxia in the estuary during summer is related to the strong stratification of the water column (Y. Cui, Wu, Ren, & Xu, 2019; H. Zhang & Li, 2010). These accumulation patterns in the PRE are more concerned with the measurement of pollutant concentrations (Tao et al., 2021), estimation of the pollutant accumulation rate (L. Zhang et al., 2009), and discussion of the sources of pollutants (Ye, Huang, Zhang, Tian, & Zeng, 2012), and lack a discussion on the understanding of accumulation spatial patterns and underlying physical control.

Methods:

Model settings are either missing or insufficiently presented. Where are the ROMS model's boundaries set? Which area do they cover? A figure with the model grid and bathymetry should be added. How much is the river discharge in the summer and how much in the winter? Please provide a sufficient summary of the model setup.

Response:

Thanks for your suggestions. Our PRE model is developed using Regional Ocean Model System (ROMs) (Shchepetkin & McWilliams, 2005). The model region covers estuary and adjacent shelf between 112.3°E-115.68°E and 20.89°N-23.13°N (Figure R9). We adopt an orthogonal grid and the resolution increases from ~1km over shelf to ~200 m inside the estuary. In vertical direction, we use the terrain-following s-ordinate (Song & Haidvogel, 1994) to discretize the water column into 30 levels. The monthly averaged river discharge data is obtained from Ministry of Water Resources of China. During summer and winter, the river discharge is approximately 30000 m³/s and 10000 m³/s, respectively. Wind forcing, heat flux, and precipitation are obtained from the ERA5 atmospheric reanalysis data by European Centre for Medium-Range Weather Forecasts (ECMWF), and they are used to force ocean circulation through the implementation of the bulk computation algorithm (Fairall, Bradley, Hare, Grachev, & Edson, 2003). The shelf current is obtained from a coarser model (Deng et al., 2022), which can cover the North South China Sea and provide the information of barotropic and baroclinic velocities, temperature, salinity, sea level along the boundaries of PRE model. Turbulent and diffusion are determined by Mellor-Yamada

2.5 turbulence-closure module (Mellor & Yamada, 1982). Eight major tidal harmonic constants (M_2 , S_2 , K_2 , N_2 , K_1 , O_1 , P_1 , Q_1) as well as the M_4 obtained from Zu, Gan, and Erofeeva (2008) are included to calculate the tidal induced current and elevation along the boundaries.

Following the reviewer's suggestions, we have integrated the above information in the revised manuscript and added Supplementary Figure R7 to introduce the seasonal river discharge and wind direction.

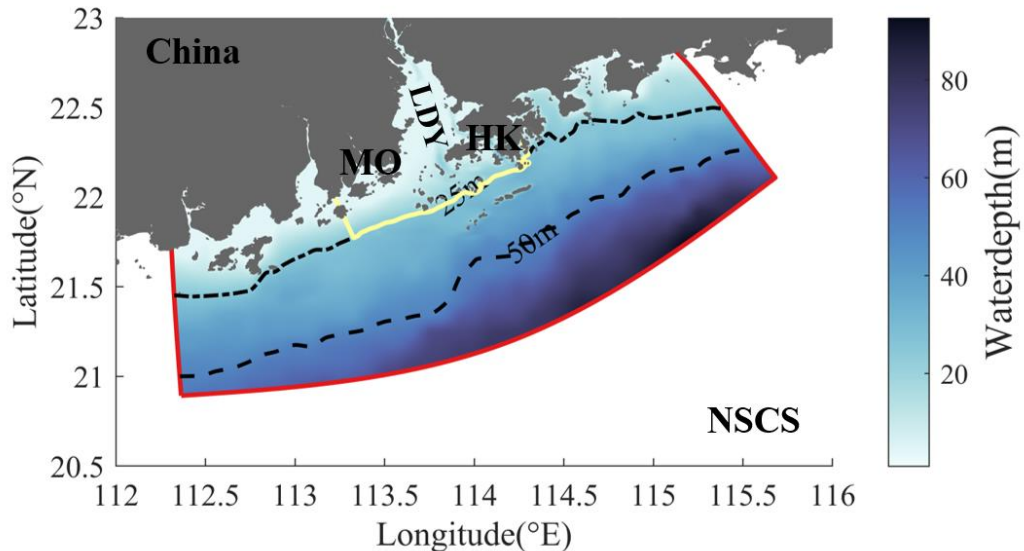


Figure R6 The bathymetry of the study area. The black dotted and dashed lines represent the isobath of 25 m and 50 m. The yellow line defines the seaside boundary of the PRE. LDY, MO, HK, and NSCS represent Lingdingyang, Macau, Hong Kong, and the northern South China Sea, respectively. The red line represents the model boundary.

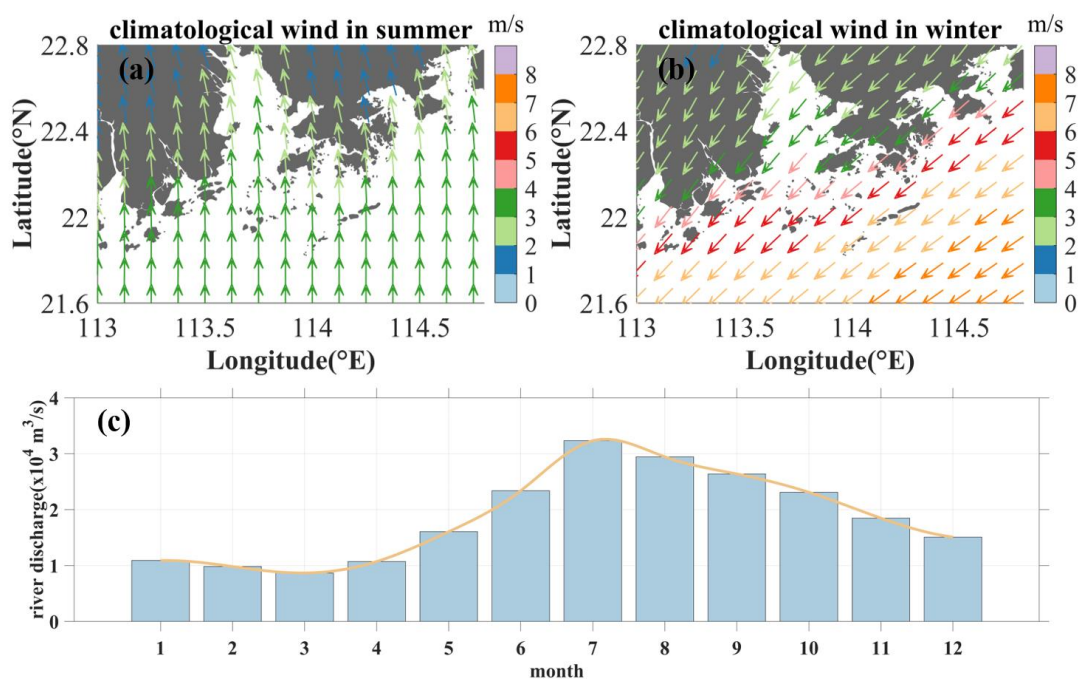


Figure R7. (a-b) The seasonal mean wind speed (m/s) during summer (June–August) and winter (December–February), respectively. (c) The monthly river discharge in the PRE.

Line 78-79 ‘Data of shelf currents were obtained by the coarser – resolution simulation’. Is there a coarser model also used? Please explain.

Response: Thank you for the comment. A well-validated coarse model simulated the shelf current covering the entire NSCS. The results provided the barotropic and baroclinic velocities, temperature, salinity, and sea level along the boundaries of the PRE. This model has been validated and used in previous investigations (L. Cui, Cai, & Liu, 2023; L. Cui, Liu, Chen, & Cai, 2024; Deng et al., 2022).

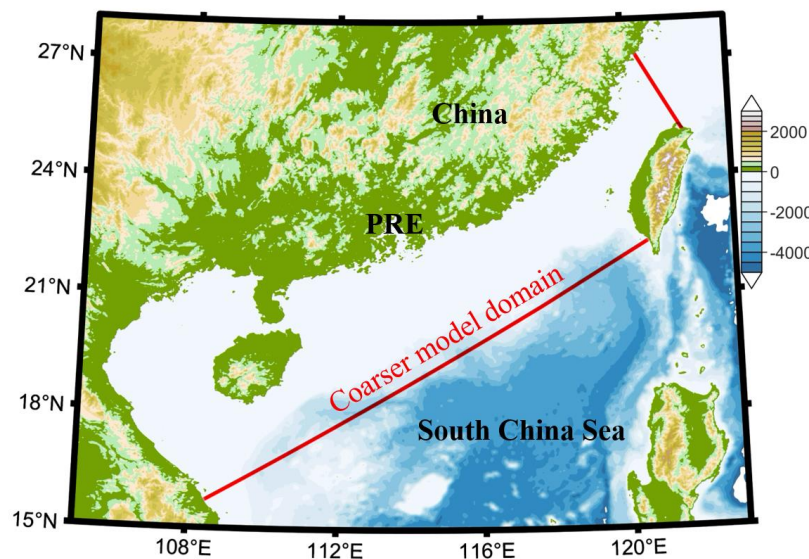


Figure R8. The domain of coarser model.

Line 88 Has the model been validated?

Response: Yes, although this model was established using climatological forcing to obtain the main features of circulation, we carefully validated the simulation of the hydrodynamic properties against data from both satellite remote sensing and long-term observations. The seasonal sea surface temperature from remote sensing and the simulation showed that the simulation captured the basic distribution and magnitude of SST (Figure R9). Considering the uncertainties in coastal salinity from remote sensing, long-term (2000-2019) observed hydrodynamic data at the SM19 station near Hong Kong were used to validate that the model accurately captured the seasonal variability of the hydrodynamic features (Figure R10).

For the basic circulation pattern, the simulation accurately reproduced the major features. In summer, an eastward shelf current established over the shelf of the Pearl River Estuary, with the onshore invasion of colder (and saltier) shelf water, is extensively intensified in the coastal seas east of the PRE (Figure 3a, b in the original manuscript). In winter, when the stronger monsoonal northeasterly wind prevailed over the study area, the coastal waters east of the PRE became much colder and mixed much better in the water column (Figure 3c, d in the original manuscript). These features are similar to those of previous investigations in this area (e.g., Cai, Liu, Liu, and Gan (2022); Z. Liu et al. (2020)), and the results from this model were successfully used in previous investigations, which provided indirect support for the

quality of the results.

In the revised manuscript, we have explained the model validation and put Figure R9, 10 in the Supplementary Material.

Line 118-121: “This model, primarily based on climatological data, was carefully verified using satellite remote sensing and long-term observations to ensure an accurate representation of the hydrodynamic properties (Fig. S2, 3). Generally, the model captures the seasonal features of circulation in this region and has been used in previous studies (Cai et al., 2022; Chu et al., 2022a; L. Cui et al., 2024).”

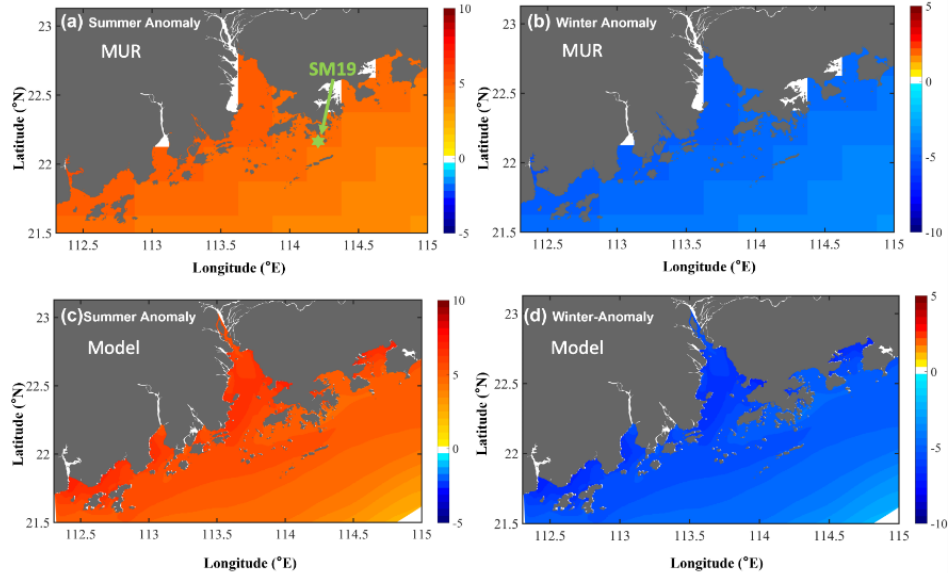


Figure R9. (a-b) Climatological SST anomaly during summer and winter from MUR SST reanalysis product from the Jet Propulsion Laboratory (JPL) of NASA (2002-2021). (c-d) are the same as (a-b) but for the model results.

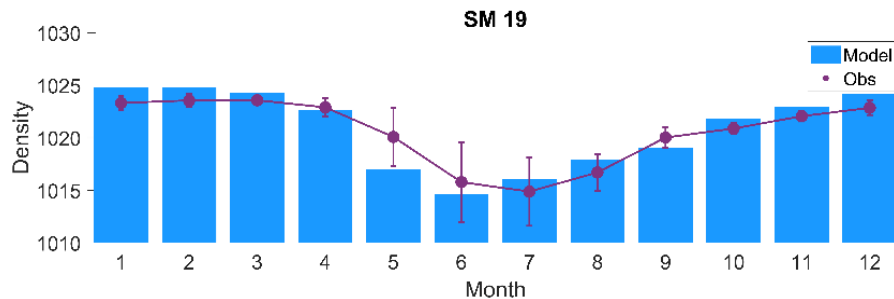


Figure R10. Time series of the surface simulated and observed potential water densities at the SM19 station near Hong Kong (https://cd.epic.epd.gov.hk/EPICRIVER/marine/?lang=zh_cn). The observed data at SM 19 from 2000-2019 was used to obtain the climatological monthly mean density, and the error bar indicates the density of STDs for each month in 20 years. The location of SM19 is shown in Figure R9a.

Line 90 Please state the implemented diffusion coefficients.

Response: The diffusion coefficient was calculated using the hydrodynamic model through the Mellor-Yamada 2.5 turbulence-closure scheme (Mellor & Yamada, 1982), which has been widely used in coastal simulations (Choi, Park, Choi, Jung, & Kim, 2021; J. Liu, Lu, & Li, 2019; Robertson & Hartlipp, 2017).

The diffusion coefficient was determined by solving the prognostic equations for the turbulent kinetic energy, turbulent kinetic energy dissipation rate, and turbulent length scale, which vary spatially and temporally within the study area.

We clarify this in the revised manuscript:

Line 104-106: “Vertical turbulence and diffusion coefficient are determined by the Mellor-Yamada 2.5 turbulence-closure module (Mellor & Yamada, 1982), which provides the turbulent mixing coefficient.”

Line 100 It is understood from Figure 3 that the calculations are in 3D, what is the vertical dimension of the grids?

Response: In our model calculations, we used the terrain-following s-ordinate (Song & Haidvogel, 1994) to discretize the water column into 30 levels, and a higher resolution for both the surface and bottom boundary layers was designed to capture the motions better there. Using the calculated 3D velocities from the hydrodynamical model, we explored accumulation dynamics in both the surface and bottom layers of the PRE.

In the revised manuscript, we clarify the vertical dimension of the grid:

Line96-97: “In the vertical direction, we used the terrain-following S-ordinate (Song & Haidvogel, 1994) to discretize the water column into 30 levels.”

Results and Discussion:

Line 145-146 Hypoxia can be common in microtidal estuaries such as the PRE or the Mississippi (see for example Schiller et al.2011) and is usually associated with stratification induced by river flows in the absence of significant mixing. It would be interesting to see the density at the surface in Figure 6 for both summer and winter in addition to the bottom ones. I presume this would show strong stratification during the summer.

Response: Following the reviewer’s suggestion, we plotted the surface density during both summer and winter. As mentioned by the reviewer, during summer, stratification occurred over the estuary with a lower surface density (Figure R11). As reported in previous studies, stratification affects the vertical diffusion of dissolved oxygen, which is a crucial factor in hypoxia (Y. Cui et al., 2019). H. Zhang and Li (2010) revealed that stratification is one of the main motivations for hypoxia in the western shoal and Hong Kong waters in the PRE during the summer.

In winter, under weaker river discharge and a robust northeasterly monsoon, the density difference between the bottom and surface water is relatively small. Stratification was reduced, and the water column was relatively well mixed (Dong et al., 2004).

We explain the stratification during summer-time and its influences on hypoxia:

Line 67-68: “The high frequency of hypoxia in the estuary during summer is related to the strong stratification of the water column (Y. Cui et al., 2019; H. Zhang & Li, 2010).”

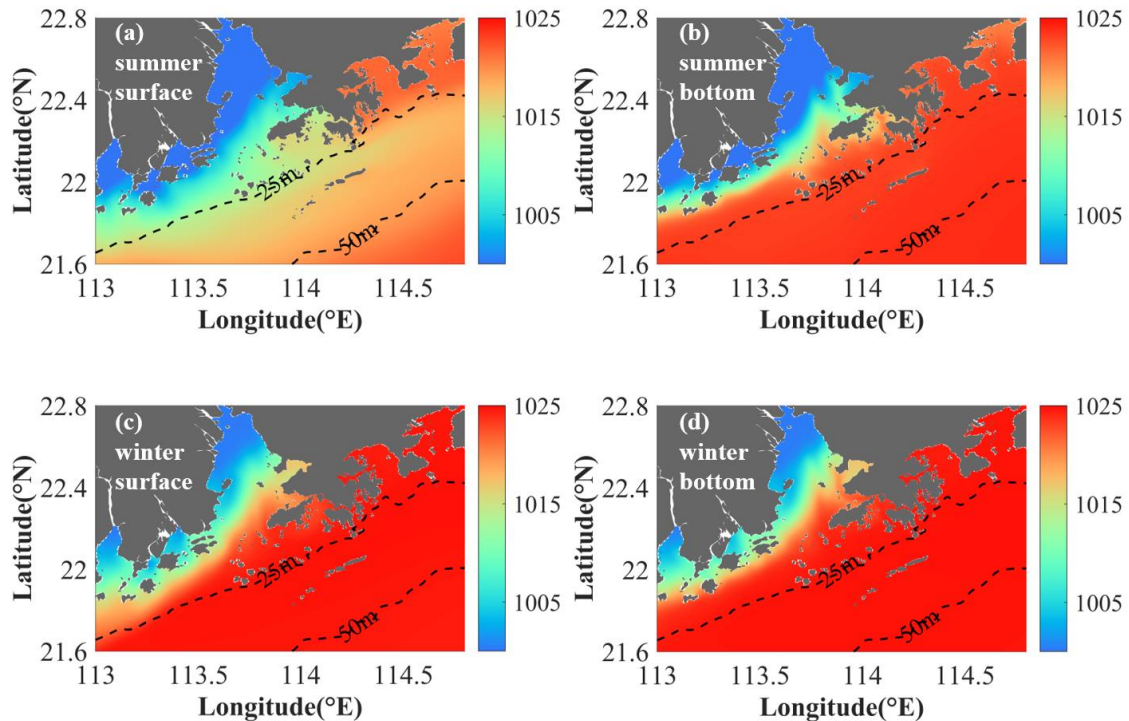


Figure R11. The density distribution in the PRE, the unit of density, is kg/m^3 .

Line 148 and 200-212. The role of the gravitational circulation is a bit obscure from the figures. A comparison between Figure 3 b and d shows that the flow arrows at the bottom do not differ much. In fact, the flow field is very similar. In addition, the density field at the bottom is also very similar between summer and winter if we compare Figure 6 a and b. This is not unusual. See for example the paper by Wong et al. (2003) which also talks about the PRE. They mention that the bottom salinity front between summer and winter is similar which basically agrees with what we see in Figure 6. Figure 3d shows an increase of the accumulation in the upper estuary in the winter compared to the summer (Figure 3b). Regarding the similar density fronts, how certain is it that the gravitational circulation is responsible for this increase? Figure 5b indicates that the increase of accumulation in the upper estuary is caused by convergence (difference between Figure 5 a and b). Could this be related to the decrease of river discharges?

Response: Thanks! According to the AB transect in the standard case (Figure R2 a-b), an obviously strengthened landward current was observed at the bottom, which was beneficial for intensifying the bottom intrusion. Summer has much more river discharge than winter in the PRE (Harrison et al., 2008), and a strong outflow pushes the water to the lower estuary and hinders the intrusion of water into the estuary. In winter, less river discharge has a weaker resistance to intrusion water, which causes strengthened landward movement of the bottom water and pushes the isopycnals to move into the inner estuary. Thus, although the front is similar, the gravitational circulation induced by river discharge contributes to changes in water accumulation in the estuary. And the increased accumulation in the upper estuary is also related to the decrease of river discharge.

Line 164 It would be helpful to add in Figure 4 a picture of the original (starting) distribution of the particles.

Response: Thank you for the comment. Initially, the particles were located in the release regions; that is,

the arrival region was the same as the release region. According to the Line 141 in the manuscript, the initial distribution D^{t_0} is $D^{t_0} = [1, 1, 1, \dots, 1]$, which represents that the original distributions of the particles are all on the diagonal location of the matrix (Figure R12):

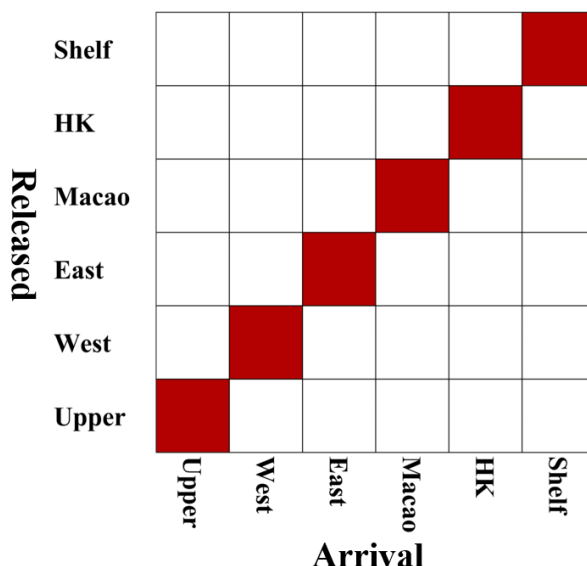


Figure R12. The location of the initial particle location.

Line 180 Do u and v indicate mean over depth velocity or at the bottom layer?

Response: The bottom u and v were used to calculate the bottom divergence.

Role of Tide and River:

The main message I get from Figure 7 and 8 is a landward displacement of water accumulation when the tides are removed, and the discharge is reduced respectively. What is the cause for this? It is not very clear from the text.

Response:

Thank you for your comments. In Figure R2 and Figure R3, we present the flow field of Transect AB with the removed tidal current/reduced river discharges to show the vertical motion of the current.

As Figure R2 shows, when the tidal currents were removed, the mixing was reduced and the stratification was intensified (Pan et al., 2020), which was associated with the landward movement of density in both winter and summer. Consequently, the higher landward accumulation probabilities are related to the strengthened bottom intrusion (Figure 7a, b in the original manuscript). In Figure R3, along the estuary, when river discharges were reduced, the weakened offshore velocity and strengthened landward front in the upper estuary were associated with a higher accumulation probability.

Line 229 How is the negative anomaly defined?

Response: The anomaly was calculated as the result of sensitivity experiments minus the standard case. The negative anomaly here means that due to the reduction in river discharge/tidal currents, the accumulation was weakened, and offshore transport was strengthened.

Conclusions:

The conclusions read more like a summary. It is suggested to rewrite it so that the core messages of this work are better highlighted.

Response: Thanks for reviewers' suggestions. We have rewritten the conclusion in the revised manuscript.

Line 364-388:

In this study, the Lagrangian method and Markov Chains were applied to illustrate the accumulation trends in different PRE regions during typical monsoon seasons.

The accumulation probabilities were obtained from the Markov Chains. Generally, surface offshore transport is always quicker than that at the bottom owing to the strong offshore current and river discharge, which are related to the relatively small accumulation at the surface layer. At the bottom, a high accumulation of water appears in the lower estuary in summer and moves shoreward in winter owing to the reduced river discharge and intensified density front. Based on these accumulation patterns, we identified six subregions in the PRE: UPPER, WEST, EAST, MO, HK, and SHELF. Across the subregions, there is a negative correlation between the net divergence ($\nabla_h \vec{V}_h$) and the accumulation probability, the intensified negative $\nabla_h \vec{V}_h$ provide the favorable conditions for water accumulation. The connections between the six subregions are discussed to illustrate the transport structure in the PRE. During summer, WEST and MO, with substantial net negative divergence and strong fronts, are powerful accumulation targets that attract particles from almost the entire estuary. The EAST and HK waters show a westward motion and are transported to the western estuary. In winter, the accumulated regions showed self-correlations, and particles were more likely to remain in the original regions. The UPPER becomes a major accumulation region owing to the blocking of the density front and the largely decreased river discharge. HK waters are transported to almost the entire estuary, contributing mainly to the accumulation in the WEST regions under westward currents.

Sensitivity experiments were conducted to evaluate the effects of tidal currents and river discharge on accumulation patterns. Generally, tidal currents and river-induced gravitational circulation affect accumulation in different ways and affect different regions of the estuary. Their joint effects controlled the accumulation pattern. Tide currents promote accumulation in the WEST and UPPER regions during winter and in the MO and HK regions during summer through increased density stratification and changes in water column mixing (Fig. 15). Increased river discharge is conducive to seaside transport in the UPPER and WEST regions during summer and in the HK region during winter, which is related to the intensified offshore current and seaward movement of the density. With the removal of tidal currents and reduced river discharges, the intensified landward current and westward transport current from HK waters and the adjacent shelf will accelerate bottom-water intrusion from the lower estuary into the upper estuary.

Figures:

Figure 1 Put panel names a and b on the left and right image. Change the colour of 50m isobath to something more visible.

Response: Thanks for reviewers' suggestion. We have modified Figure 1 in the revised manuscript.

Figure 3. Use a different colorscale for the vectors (e.g., blue), differences can hardly be spotted with this one. Add an arrow size. Same for the colour of the areas' names. Why do you show results at the surface

only in this occasion and nowhere else? Is your research focusing on the bottom or the entire water column?

Response: Thanks for reviewers' suggestions! We will separate the information of flow field from Figure 3 in the original manuscript and get the new version of flow field as Figure R13.

Under the strong offshore current, the accumulation probability on the surface is much weaker than bottom layer. The bottom layer has slower offshore motions and most environmental problems such as hypoxia and heavy metal enrichment occurred mainly in the bottom as well. Therefore, we choose the bottom layer to discuss the internal connection and accumulation dynamics between different regions in the PRE, which can show the pattern more clearly. Following discussion on the accumulation dynamics are focused on the bottom layer.

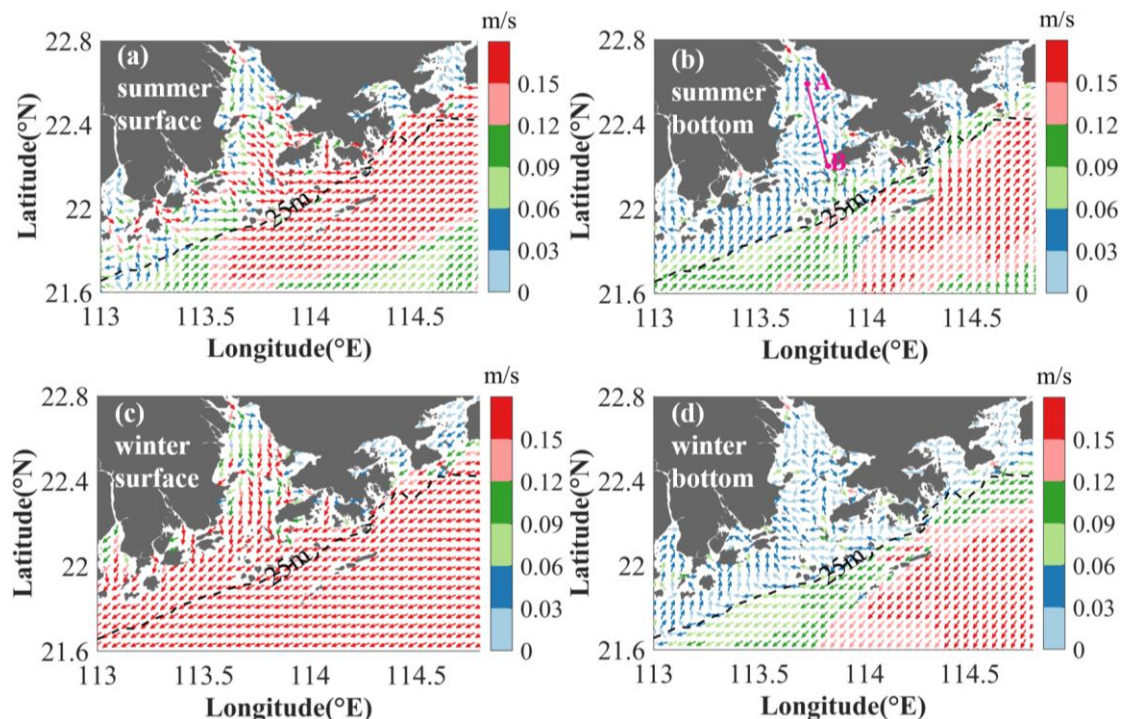


Figure R13: (a–b) The flow field of the standard case at the surface layer and bottom layer during summertime, respectively. (c–d) are the same as (a–b), but for winter time.

Figure 5. Keep the y axis scale equal between a and b for better comparison.

Response: We use the same y axis scale here to show the distinction.

Figure 6. Add results for the surface layer.

Response: The density gradient of surface layer is shown as follow:

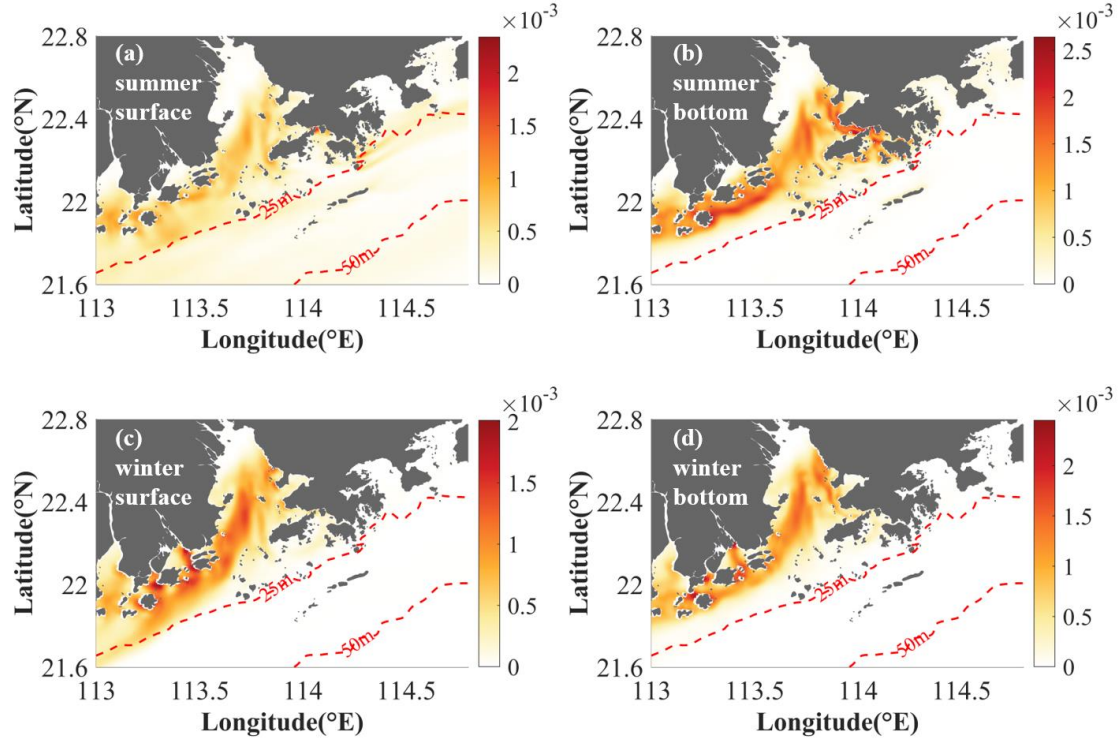


Figure R14. The density front (kg/m^3) on the surface layer (a) and bottom layer (b) during summer time, while (c-d) are same as (a-b) in winter.

Figure 7. Are these results given for the entire water column or just the bottom? Make y axis equal between c and d.

Figure 8. Same comments as in Figure 7.

Response: Thanks for reviewers' suggestions! The results in Figure 7 are focused on the bottom layer. Compared to the bottom layer, particles on surface layer leave the estuary quickly without significant accumulation effects. Thus, the discussion on hydrodynamic control in this paper are mainly concentrated on the bottom layers. We will make y axis scale keep same like Figure R15, 16.

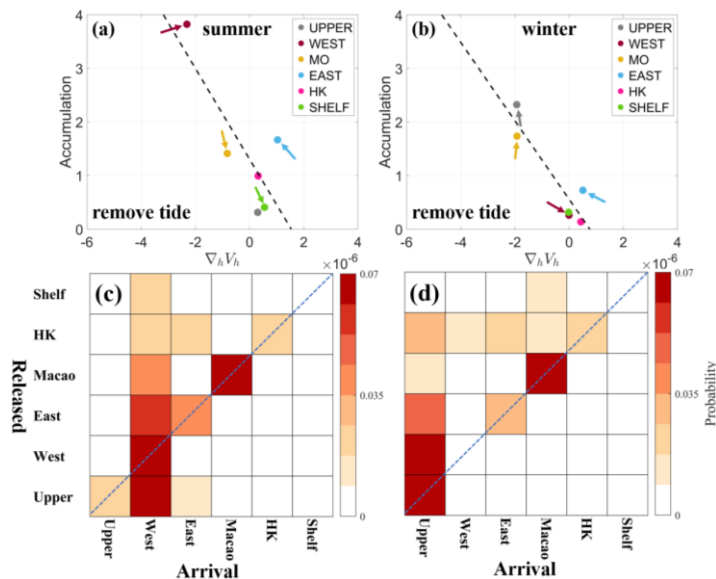


Figure R15: (a-b) Scatter plot of accumulation probability against $\nabla_h \vec{V}_h$ for various subregions during summer and winter in removing tide cases. The arrow represents the changes of $\nabla_h \vec{V}_h$ and accumulation due to the removing of

tide in each subregion. (c-d) The connection between six regions for removal of tidal current at the bottom layer during summer and winter time, respectively.

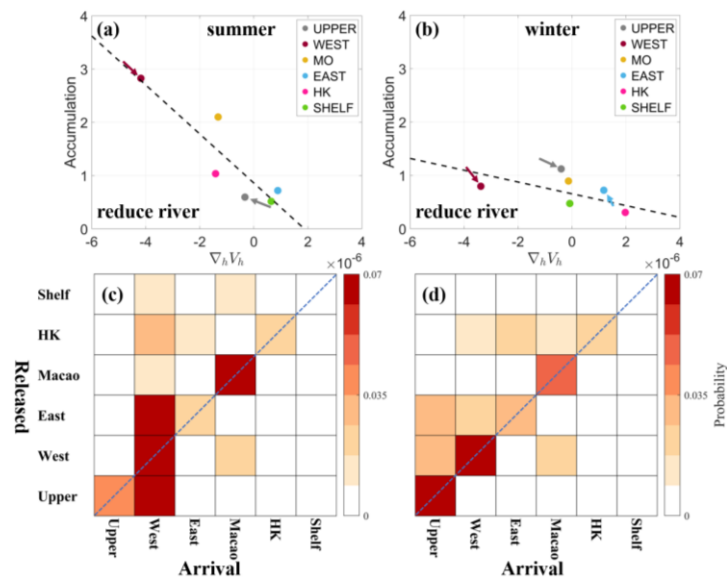


Figure R16: (a-b) Scatter plot of accumulation probability against $\nabla_h \vec{V}_h$ for various subregions during summer and winter in river-reduced cases. The arrow represents the changes of $\nabla_h \vec{V}_h$ and accumulation due to the reduction of discharge in each subregion. (e-f) The connection between six regions for the case with reduced river discharge.

References

Acha, E. M., Mianzan, H. W., Iribarne, O., Gagliardini, D. A., Lasta, C., & Daleo, P. (2003). The role of the Río de la Plata bottom salinity front in accumulating debris. *Marine pollution bulletin*, 46(2), 197-202. doi:[https://doi.org/10.1016/S0025-326X\(02\)00356-9](https://doi.org/10.1016/S0025-326X(02)00356-9)

Ascione Kenov, I., Garcia, A. C., & Neves, R. (2012). Residence time of water in the Mondego estuary (Portugal). *Estuarine, coastal and shelf science*, 106, 13-22. doi:10.1016/j.ecss.2012.04.008

Balachandran, K. K., Lalu Raj, C. M., Nair, M., Joseph, T., Sheeba, P., & Venugopal, P. (2005). Heavy metal accumulation in a flow restricted, tropical estuary. *Estuarine, coastal and shelf science*, 65(1), 361-370. doi:<https://doi.org/10.1016/j.ecss.2005.06.013>

Banas, N. S., & Hickey, B. M. (2005). Mapping exchange and residence time in a model of Willapa Bay, Washington, a branching, macrotidal estuary. *Journal of Geophysical Research*, 110(C11), C11011-n/a. doi:10.1029/2005JC002950

Cai, Z., Liu, G., Liu, Z., & Gan, J. (2022). Spatiotemporal variability of water exchanges in the Pearl River Estuary by interactive multiscale currents. *Estuarine, coastal and shelf science*, 265, 107730. doi:10.1016/j.ecss.2021.107730

Callahan, J., Dai, M., Chen, R. F., Li, X., Lu, Z., & Huang, W. (2004). Distribution of dissolved organic matter in the Pearl River Estuary, China. *Marine chemistry*, 89(1), 211-224. doi:<https://doi.org/10.1016/j.marchem.2004.02.013>

Choi, Y., Park, Y., Choi, M., Jung, K. T., & Kim, K. O. (2021). A Fine Grid Tide-Wave-Ocean Circulation Coupled Model for the Yellow Sea: Comparison of Turbulence Closure Schemes in Reproducing Temperature Distributions. *Journal of Marine Science and Engineering*, 9(12), 1460. Retrieved from <https://www.mdpi.com/2077-1312/9/12/1460>

Chu, N., Liu, G., Xu, J., Yao, P., Du, Y., Liu, Z., & Cai, Z. (2022). Hydrodynamical transport structure and lagrangian connectivity of circulations in the Pearl River Estuary. 9. doi:10.3389/fmars.2022.996551

Cui, L., Cai, Z., & Liu, Z. (2023). Water exchange and transport pathways in estuary-shelf region of Pearl River Estuary under multiple forcings. *Continental shelf research*, 266, 105099. doi:10.1016/j.csr.2023.105099

Cui, Y., Wu, J., Ren, J., & Xu, J. (2019). Physical dynamics structures and oxygen budget of summer hypoxia in the Pearl River Estuary. *Limnology and Oceanography*, 64(1), 131-148. doi:<https://doi.org/10.1002/limo.11025>

Deng, Y., Liu, Z., Zu, T., Hu, J., Gan, J., Lin, Y., . . . Cai, Z. (2022). Climatic Controls on the Interannual Variability of Shelf Circulation in the Northern South China Sea. *Journal of Geophysical Research: Oceans*, 127(7), e2022JC018419. doi:<https://doi.org/10.1029/2022JC018419>

Dong, L., Su, J., Ah Wong, L., Cao, Z., & Chen, J.-C. (2004). Seasonal variation and dynamics of the Pearl River plume. *Continental shelf research*, 24(16), 1761-1777. doi:10.1016/j.csr.2004.06.006

Fairall, C. W., Bradley, E. F., Hare, J., Grachev, A. A., & Edson, J. B. (2003). Bulk parameterization of air-sea fluxes: Updates and verification for the COARE algorithm. *Journal of climate*, 16(4), 571-591.

Gong, W., Shen, J., & Hong, B. (2009). The influence of wind on the water age in the tidal Rappahannock River. *Marine Environmental Research*, 68(4), 203-216. doi:<https://doi.org/10.1016/j.marenvres.2009.06.008>

Harrison, P. J., Yin, K., Lee, J. H. W., Gan, J., & Liu, H. (2008). Physical–biological coupling in the Pearl River Estuary. *Continental shelf research*, 28(12), 1405-1415. doi:<https://doi.org/10.1016/j.csr.2007.02.011>

He, C., Yin, Z.-Y., Stocchino, A., & Wai, O. W. H. (2023). Generation of macro-vortices in estuarine compound channels. *Frontiers in Marine Science*, 10. doi:10.3389/fmars.2023.1082506

He, C., Yin, Z.-Y., Stocchino, A., Wai, O. W. H., & Li, S. (2022). The coastal macro-vortices dynamics in Hong Kong waters and its impact on water quality. *Ocean Modelling*, 175, 102034. doi:<https://doi.org/10.1016/j.ocemod.2022.102034>

Lam, T. W. L., Fok, L., Lin, L., Xie, Q., Li, H.-X., Xu, X.-R., & Yeung, L. C. (2020). Spatial variation of floatable plastic debris and microplastics in the Pearl River Estuary, South China. *Marine pollution bulletin*, 158, 111383. doi:<https://doi.org/10.1016/j.marpolbul.2020.111383>

Lane, R. R., Day, J. W., Marx, B. D., Reyes, E., Hyfield, E., & Day, J. N. (2007). The effects of riverine discharge on temperature, salinity, suspended sediment and chlorophyll a in a Mississippi delta estuary measured using a flow-through system. *Estuarine, coastal and shelf science*, 74(1), 145-154. doi:<https://doi.org/10.1016/j.ecss.2007.04.008>

Li, D., Gan, J., Hui, C., Yu, L., Liu, Z., Lu, Z., . . . Dai, M. (2021). Spatiotemporal Development and Dissipation of Hypoxia Induced by Variable Wind-Driven Shelf Circulation off the Pearl River Estuary: Observational and Modeling Studies. 126(2), e2020JC016700. doi:<https://doi.org/10.1029/2020JC016700>

Li, T., & Li, T.-J. (2018). Sediment transport processes in the Pearl River Estuary as revealed by grain-size end-member modeling and sediment trend analysis. *Geo-Marine Letters*, 38(2), 167-178. doi:10.1007/s00367-017-0518-2

Li, X., Lu, C., Zhang, Y., Zhao, H., Wang, J., Liu, H., & Yin, K. (2020). Low dissolved oxygen in the

Pearl River estuary in summer: Long-term spatio-temporal patterns, trends, and regulating factors. *Marine pollution bulletin*, 151, 110814-110814. doi:10.1016/j.marpolbul.2019.110814

Liu, J., Lu, S., & Li, Y. (2019). Numerical study on sensibility of turbulence closure schemes at Oujiang River Estuary. *Applied Ocean Research*, 88, 76-88. doi:<https://doi.org/10.1016/j.apor.2019.04.014>

Liu, Z., Zu, T., & Gan, J. (2020). Dynamics of cross-shelf water exchanges off Pearl River Estuary in summer. *Progress in Oceanography*, 189, 102465. doi:<https://doi.org/10.1016/j.pocean.2020.102465>

Mao, Q., Shi, P., Yin, K., Gan, J., & Qi, Y. (2004). Tides and tidal currents in the Pearl River Estuary. *Continental shelf research*, 24(16), 1797-1808. doi:10.1016/j.csr.2004.06.008

Mellor, G. L., & Yamada, T. (1982). Development of a turbulence closure model for geophysical fluid problems. *Reviews of Geophysics*, 20(4), 851-875. doi:<https://doi.org/10.1029/RG020i004p00851>

Mestres, M., Sánchez-Arcilla, A., Sierra, J. P., Möss, C., Tagliani, P., Möller, O., & Niencheski, L. (2006). Coastal bays as a sink for pollutants and sediment. *Journal of Coastal Research*, 1546-1550.

Pan, J., Lai, W., & Thomas Devlin, A. (2020). Circulations in the Pearl River Estuary: Observation and Modeling. In *Estuaries and Coastal Zones - Dynamics and Response to Environmental Changes*.

Robertson, R., & Hartlipp, P. (2017). Surface wind mixing in the Regional Ocean Modeling System (ROMS). *Geoscience Letters*, 4(1), 24. doi:10.1186/s40562-017-0090-7

Shchepetkin, A. F., & McWilliams, J. C. (2005). The regional oceanic modeling system (ROMS): a split-explicit, free-surface, topography-following-coordinate oceanic model. *Ocean modelling (Oxford)*, 9(4), 347-404. doi:10.1016/j.ocemod.2004.08.002

Song, Y., & Haidvogel, D. (1994). A Semi-implicit Ocean Circulation Model Using a Generalized Topography-Following Coordinate System. *Journal of Computational Physics*, 115(1), 228-244. doi:<https://doi.org/10.1006/jcph.1994.1189>

Tao, W., Niu, L., Dong, Y., Fu, T., & Lou, Q. (2021). Nutrient Pollution and Its Dynamic Source-Sink Pattern in the Pearl River Estuary (South China). *Frontiers in Marine Science*, 8. doi:10.3389/fmars.2021.713907

Vermeiren, P., Muñoz, C. C., & Ikejima, K. (2016). Sources and sinks of plastic debris in estuaries: A conceptual model integrating biological, physical and chemical distribution mechanisms. *Marine pollution bulletin*, 113(1-2), 7-16. doi:10.1016/j.marpolbul.2016.10.002

Wang, A.-j., Kawser, A., Xu, Y.-h., Ye, X., Rani, S., & Chen, K.-l. (2016). Heavy metal accumulation during the last 30 years in the Karnaphuli River estuary, Chittagong, Bangladesh. *SpringerPlus*, 5(1), 2079. doi:10.1186/s40064-016-3749-1

Wang, T., Zhao, S., Zhu, L., McWilliams, J. C., Galgani, L., Amin, R. M., . . . Chen, M. (2022). Accumulation, transformation and transport of microplastics in estuarine fronts. *Nature Reviews Earth & Environment*, 3(11), 795-805. doi:10.1038/s43017-022-00349-x

Wong, L. A., Chen, J. C., Xue, H., Dong, L. X., Su, J. L., & Heinke, G. (2003). A model study of the circulation in the Pearl River Estuary (PRE) and its adjacent coastal waters: 1. Simulations and comparison with observations. *Journal of Geophysical Research: Oceans*, 108(C5). doi:<https://doi.org/10.1029/2002JC001451>

Ye, F., Huang, X., Zhang, D., Tian, L., & Zeng, Y. (2012). Distribution of heavy metals in sediments of the Pearl River Estuary, Southern China: Implications for sources and historical changes.

Journal of Environmental Sciences, 24(4), 579-588. doi:[https://doi.org/10.1016/S1001-0742\(11\)60783-3](https://doi.org/10.1016/S1001-0742(11)60783-3)

Zhang, D., Zhang, X., Tian, L., Ye, F., Huang, X., Zeng, Y., & Fan, M. (2013). Seasonal and spatial dynamics of trace elements in water and sediment from Pearl River Estuary, South China. *Environmental Earth Sciences*, 68(4), 1053-1063. doi:10.1007/s12665-012-1807-8

Zhang, H., & Li, S. (2010). Effects of physical and biochemical processes on the dissolved oxygen budget for the Pearl River Estuary during summer. *Journal of marine systems*, 79(1), 65-88. doi:<https://doi.org/10.1016/j.jmarsys.2009.07.002>

Zhang, L., Yin, K., Wang, L., Chen, F., Zhang, D., & Yang, Y. (2009). The sources and accumulation rate of sedimentary organic matter in the Pearl River Estuary and adjacent coastal area, Southern China. *Estuarine, coastal and shelf science*, 85(2), 190-196. doi:<https://doi.org/10.1016/j.ecss.2009.07.035>

Zu, T., & Gan, J. (2015). A numerical study of coupled estuary–shelf circulation around the Pearl River Estuary during summer: Responses to variable winds, tides and river discharge. *Deep Sea Research Part II: Topical Studies in Oceanography*, 117, 53-64. doi:<https://doi.org/10.1016/j.dsr2.2013.12.010>

Zu, T., Gan, J., & Erofeeva, S. Y. (2008). Numerical study of the tide and tidal dynamics in the South China Sea. *Deep Sea Research Part I: Oceanographic Research Papers*, 55(2), 137-154. doi:<https://doi.org/10.1016/j.dsr.2007.10.007>

Zu, T., Wang, D., Gan, J., & Guan, W. (2014). On the role of wind and tide in generating variability of Pearl River plume during summer in a coupled wide estuary and shelf system. *Journal of marine systems*, 136, 65-79. doi:<https://doi.org/10.1016/j.jmarsys.2014.03.005>

